Title
Mechanism and kinetics of 1-dodecanol etherification over tungstated zirconia

Authors
Rorrer, Julie
He, Ying
Toste, F Dean
et al.

Publication Date
2017-10-01

DOI
10.1016/j.jcat.2017.08.001

Peer reviewed

Journal of Catalysis 354 (2017) 13–23

Contents lists available at ScienceDirect

Journal of Catalysis

journal homepage: www.elsevier.com/locate/jcat

Mechanism and kinetics of 1-dodecanol etherification over tungstated zirconia

Julie Rorrer [a,b], Ying He [a,c], F. Dean Toste [a,c], Alexis T. Bell [a,b,*]

[a] Energy Biosciences Institute, University of California Berkeley, CA 94720, United States
[b] Department of Chemical and Biomolecular Engineering, University of California Berkeley, CA 94720, United States
[c] Department of Chemistry, University of California Berkeley, CA 94720, United States

ARTICLE INFO

Article history:
Received 3 June 2017
Revised 2 August 2017
Accepted 3 August 2017
Available online 23 August 2017

Keywords:
Dodecanol
Etherification
Tungstated zirconia
Di-dodecylether
Dodecene

ABSTRACT

Growing interest in finding renewable alternatives to conventional fossil fuels and petroleum-derived specialty chemicals has motivated the investigation of biomass-derived alcohols to make ethers as diesel additives or lubricants. To optimize the direct etherification of long chain alcohols in the liquid phase, it is necessary to develop an understanding of the kinetics and mechanism of etherification and dehydration reactions. In this study, tungstated zirconia was identified as a selective solid-acid catalyst for the liquid-phase etherification of 1-dodecanol. Investigations of the mechanism and kinetics of this reaction suggest that cooperation between Brønsted- and Lewis-acid sites on tungstated zirconia enhances the selectivity to ether by increasing the surface concentration of adsorbed alcohol, thereby promoting bi-molecular ether formation relative to unimolecular alcohol dehydration. The suggested rate limiting step for etherification is the formation of a C—O bond between two adsorbed alcohol molecules, and the suggested rate-limiting step for dehydration is the cleavage of the C—H bond of the β-carbon atom in an adsorbed alcohol. Measurements of the kinetic isotope effects for etherification and dehydration support the proposed mechanism. A microkinetic model based on the proposed mechanism for dodecanol etherification and dehydration over tungstated zirconia accurately describes the observed effects of alcohol concentration and product inhibition.

1. Introduction

Continued use of fossil energy resources to produce fuels contributes to an increase in atmospheric CO_2 and in turn to changes in the global climate [1]. This concern has motivated the exploration of biomass as a possible source of renewable carbon for the production of fuels and lubricants [2]. A central question is how to convert biomass into synthons that could be used to produce fuels and lubricants. One of the appealing approaches is to ferment the sugars derived by hydrolysis of cellulose and hemicellulose into alcohols such as ethanol and butanol. The condensation of furfural with acetone under hydrogen can also produce 1-octanol [3]. Other longer-chain alcohols such as 1-dodecanol can be produced by hydrolysis of triglycerides and fatty acids. These linear alcohols can also be converted to higher carbon-number alcohols with branched carbon chains via the Guerbet reaction, and the corresponding Guerbet alcohols can be converted to ethers [4].

Ethers are attractive products because they can be used as diesel additives and automotive lubricant base oils. Diesel-range linear ethers produced from biomass are of interest because they have high cetane numbers as well as high energy density [5–8]. Shorter chain branched ethers have high octane numbers and can be added to gasoline [9]. Ethers are also of interest as lubricants. For example, alkylated di-phenyl ether and glyceryl ethers have excellent properties [10,11], and branching in the alkyl portions of ethers lowers the pour points and raises the viscosity of the ether [12,13]. Therefore, ether-based lubricants sourced from biomass provide a stable, tunable, and renewable alternative to poly-alpha-olefins produced from petroleum [14,15].

Ethers can be prepared either by direct, acid-catalyzed etherification of alcohols, or by reductive etherification of an alcohol and an aldehyde or ketone. Direct etherification of alcohols is advantageous because it does not require the use of hydrogen and precious metal catalysts for reduction [16]. The competing reaction in the presence of an acid catalyst is alcohol dehydration to produce the corresponding alkene, a process that is favored thermodynamically at temperatures above approximately 350 K. Since higher temperatures are desirable for increasing reaction rates, this raises

* Corresponding author at: Energy Biosciences Institute, University of California Berkeley, CA 94720, United States.
E-mail address: alexbell@berkeley.edu (A.T. Bell).

http://dx.doi.org/10.1016/j.jcat.2017.08.001
0021-9517/

the question of how one can favor etherification over alkene formation.

Selective etherification has been reported for the liquid-phase reactions of 1-octanol, 1-hexanol, and 1-pentanol over acid catalysts such as Amberlyst 70 [17,18], Nafion NR-50 [18,19], and H-BEA zeolite [20]. While polymeric resins are selective to ether, they are not as thermally stable as metal oxides [18,21]. Zeolites, on the other hand, are thermally stable, but catalyze unwanted side products and deactivate due to coking [22].

In this study, we screened a series of solid-acid catalysts for the direct etherification of 1-dodecanol and identified tungstated zirconia as a highly active and selective catalyst. Tungstated zirconia has been employed previously for acid-catalyzed reactions including gas-phase isomerization of n-butane [23], gas-phase dehydration of alcohols to alkenes [24], and liquid-phase reactions, such as esterification, transesterification, and alkylation [24–26]. Investigations of the gas-phase kinetics for the dehydration of short-chain, linear alcohols over tungstated zirconia indicate that dehydration occurs via a unimolecular mechanism but that these alcohols are not converted to ethers [27,28]. By contrast, we found that the etherification of dodecanol in the liquid phase is highly selective over tungstated zirconia. Motivated by this finding, we undertook an investigation of the mechanism and kinetics of the etherification and dehydration of 1-dodecanol over tungstated zirconia with the objective of developing an explanation for the high selectivity of this catalyst for etherification in the liquid phase.

2. Materials and methods

2.1. Materials

All chemicals obtained commercially were used without further purification. The following compounds were obtained from Sigma-Aldrich: 1-hexanol (>98%), 1-dodecanol (>98%), decane (>95%), dodecane (>99%), hexane (>99%), 1-hexene (>99%), and pyridine (99.8%). N-tetradecane was obtained from Spectrum Chemical (>99%), and was used as an internal standard for analytical purposes. Di-dodecyl ether (>95%) and 1-dodecene (>95%) were obtained from TCI. Di-n-hexyl ether (>98%), and 2,6-di-tert-butylpyridine (97%) were obtained from Alpha Aesar. Hexan-1,1-d_2-1-ol (>99%) was obtained from CDN Isotopes Inc. Hexan-2,2-d_2-1-ol was synthesized and purified to >98% according to Ref. [29] Amberlyst 15 (hydrogen form, dry), and Amberlyst 36 were obtained from Sigma-Aldrich. Amberlyst 70 was obtained from Dow Chemical, and was dried at 368 K and stored in a desiccator before use. Zeolite BEA was obtained from Alpha Aesar, and was calcined at 873 K for 6 h before use. Gamma-alumina was obtained from Strem Chemicals. Mesostructured silica (MCM-41 hexagonal type), Nafion NR-50, and mesostructured aluminosilicate (MCM-41, hexagonal) were obtained from Sigma-Aldrich. Para-toluene sulfonic acid was obtained from Spectrum Chemical.

2.2. Synthesis of zirconia and tungstated zirconia

Porous amorphous zirconia, monoclinic zirconia, and tungstated zirconia were synthesized using previously reported methods.[23,30,31] Amorphous zirconium oxyhydroxide ($ZrO_x(OH)_{4-2x}$) was formed by adding ammonium hydroxide (Spectrum, 28–30%) dropwise to a stirred solution of 0.5 M zirconyl chloride octahydrate (Sigma Aldrich, 98%) at 298 K. The precipitate was filtered and rinsed with 10% ammonium hydroxide and dried at 383 K for 24 h. Tungstated zirconia (4.1, 7.7, 10.2, 12.6, 15.4, 22.3 wt% W) was prepared via incipient wetness impregnation of amorphous zirconium oxyhydroxide with aqueous ammonium metatungstate hydrate (Spectrum). After impregnation, all catalysts were heated at 10 K/min and treated in air at 1073 K for 3 h, then cooled to room temperature. To prepare pure zirconia, amorphous zirconium oxyhydroxide was calcined at 1073 K under the same incipient wetness impregnation conditions but without the addition of ammonium metatungstate. Each catalyst was then crushed to <250 μm mesh using a mortar and pestle.

2.3. Catalyst characterization

Powder X-ray diffraction (XRD) patterns for WO_x/ZrO_2 (0–22 wt % W) were taken with a Bruker D8 GADDS diffractometer equipped with a Cu−Kα source (40 kV, 40 mA). Raman spectra were obtained with a LabRAM HR Horiba Scientific Raman spectrometer equipped with a 633 nm^{-1} laser. BET surface area measurements were performed with a Micrometrics TriStar BET and pretreated with a Micrometrics FlowPrep 060. Brønsted- and Lewis-acid sites were identified and the ratio of these sites was determined from IR spectra of adsorbed pyridine. Spectra were acquired using a Thermo Scientific Nicolet 6700 Fourier Transform Infrared Spectrometer (FT-IR) equipped with a Diffuse Reflectance Infrared Fourier Transform Spectroscopy (DRIFTS) cell. A mixture of catalyst (50 mg) diluted with KBr (250 mg) was added to the DRIFTS cell and pretreated at 573 K for 2 h under helium. Background scans of the catalyst were taken at 393 K, 423 K, 473 K, 523 K, and 573 K. Pyridine was introduced into the He flow at 393 K, and spectral data was taken after stabilization of adsorbed pyridine at 393 K. The temperature was then raised to measure the amount of pyridine that remained adsorbed at 423 K, 473 K, 523 K, and 573 K. Spectral intensities were calculated using the Kubelka-Munk function. The concentration of Brønsted-acid sites was determined by titration with NH_4OH. The protons on the catalysts were first exchanged for Na^+ cations by placing the catalyst in a 1 M NaCl solution overnight, and then the solution was titrated with NH_4OH until the pH was neutral, using phenolphthalein as an indicator. The moles of base added was used as a metric for the number of H^+ ions in solution [32]. ICP Elemental analysis was performed by Galbraith Laboratories, Inc. in order to determine tungsten weight loadings.

2.4. Isotopic labeling and NMR

Isotopic labeling of the alpha and beta hydrogen atoms in 1-hexanol was used to support the proposed mechanisms of etherification and dehydration. Hexan-2,2-d_2-1-ol was prepared according to literature and the structure was confirmed using ^1H NMR [29]. Kinetic isotope effects (k_H/k_D) were determined by measuring the initial rates of alkene and ether formation for 1-hexanol, hexan-1,1-d_2-1-ol, and hexan-2,2-d_2-1-ol. NMR spectra of the reaction products were recorded with a Bruker AVQ-400 spectrometer.

2.5. Batch reactions

All reactions were carried out in sealed 12 mL Q-Tube batch reaction vessels with magnetic stirring at 600 RPM using an IKA C-MAG HS 10 digital hot plate with temperature control accurate to within ±1 K. For determination of the reaction kinetics, a separate batch reaction was carried out for each time point to ensure consistency of volume and concentration of each sample. All reactions over tungstated zirconia were carried out either in the absence of solvent or in decane with 100 mg of catalyst and 250 μL of dodecanol (unless otherwise noted). N-tetradecane (100 μL) was added post-reaction as a standard for analysis. The reactants and catalyst were added to the Q-Tube in the preheated hot plate with an aluminum heating block, and after the specified reaction time, the vials were removed from the hot plate and placed in an ice bath to stop the reaction. Products were diluted with 5 mL of acetone, and centrifuged at 4000 RPM for

8 min to remove the catalyst. A 200 μL aliquot of this solution was then diluted with another 1.3 mL of acetone and added to a GC vial for analysis with gas chromatography and mass spectrometry.

2.6. Product analysis

Product analysis was carried out using a Varian CP-3800 Gas Chromatograph/Mass Spectrometer (GC/MS). The products were detected using a flame ionization detector (FID) to ensure high a signal to noise ratio, and were identified using the Varian 320 triple quadrupole mass spectrometer (MS). N-tetradecane was used as an internal standard to ensure accurate product quantification. FID response factors were determined using commercially purified compounds. For all reactions, the main products observed were ether, alkenes, and water. At longer reaction times, trace amounts of branched ether and oligomerized olefins were detected, but were considered to be negligible. Mass balances for all reactions were achieved to within ±5%, with the assumption that one mole of water is formed for every mole of ether or alkene formed.

2.7. Analysis of reaction kinetics

Initial rates of etherification and dehydration of 1-dodecanol were determined by measuring the initial rates of formation of ether and alkene. Individual batch reactions for each time point were carried out at each temperature over the temperature range of 388–403 K. Mass transfer limitations for linear alcohols were found to be negligible at 600 RPM for catalyst particle sizes less than 250 μm in diameter (Supporting Information, Fig. S1).

3. Results and discussion

3.1. Catalyst selection

A number of solid-acid catalysts were screened for the liquid-phase etherification of 1-dodecanol because of their excellent stability and recoverability. Table 1 summarizes the results of these experiments, which were carried out at 393 K and low alcohol conversions (<15%), for which the inhibiting effects of products on catalytic activity and selectivity are negligible [28]. Amberlyst 70, Nafion NR-50, and WO_x/ZrO_2 (12.6 wt% W) exhibited the highest ether selectivities (97%, 98%, and 94%, respectively). Amberlyst 70 is a Brønsted-acidic styrene–divinylbenzene resin with a high density of sulfonic acid groups, and Nafion NR-50 has Brønsted-acidic sulfonic acid groups enhanced by an electron-withdrawing polyfluorocarbon backbone [18,21]. While Amberlyst 70 and Nafion NR-50 are highly selective to ether, they are unstable above 463 K [18,21]. The high thermal stability of tungstated zirconia is advantageous since the catalyst can be readily regenerated through re-calcination in air, eliminating the need for solvents such as toluene required for resin regeneration [33]. In addition, resins such as Nafion NR-50 are known to swell in the reaction medium, thereby introducing inconsistent mass transfer limitations due to variation in the number of accessible acid sites with time [33]. Because of its high activity, thermal stability, and selectivity, WO_x/ZrO_2 (12.6 wt% W) was selected for further investigation.

3.2. Catalyst characterization

Fig. 1a and b show X-ray Diffraction (XRD) and Raman spectra for different weight loadings of WO_x/ZrO_2. For low weight loadings of tungstated zirconia, the zirconia exists primarily in the monoclinic phase. From the XRD in Fig. 1a, the 0 wt% W sample (i) has peaks at 2θ angles of 24°, 28°, 32°, and 56°, which are characteristic of monoclinic zirconia [26,30,34]. These peaks can also be observed for the 4 wt% W sample (ii). As the weight loading increases, features for tetragonal zirconia become predominant, as evidenced by the XRD peaks at 2θ angles of approximately 30°, 35°, 50°, and 59° for the 4–22 wt% catalysts [30,34,35]. The presence of tetragonal zirconia has been attributed to tungsten oxide inhibition of zirconia sintering and transformation to the monoclinic phase during calcination [24,36]. When the weight loading of tungsten oxide becomes high enough to completely cover the surface of the zirconia (v-vii), bulk tungsten oxide is formed, as evidenced by the presence of XRD peaks at 2θ angles between 23° and 25° [37].

The Raman spectra for the catalysts are shown in Fig. 1b. Spectrum (i) exhibits bands at 178–220, 307–379, and at 635 cm^{-1}, which confirm that the zirconia is monoclinic [38]. As the tungsten oxide weight loading increases, a small band appears at 1020 cm^{-1}. This band has been attributed to terminal W═O bonds, characteristic of oligomeric tungsten oxide species [26]. At weight loadings above 10.2 wt% W (spectrum (iv)), bands at 274, 715, and 807 cm^{-1} appear that are characteristic of the W—O bond stretches for bulk WO_3 [39]. For the 12.6 wt% tungstated zirconia, it is estimated that the Lewis-acid sites on the surface are predominantly due to W because the exposed Zr has been covered.

Fig. 2a shows the relationship between W weight loading and Brønsted-acid site density. The surface concentration of Brønsted-acid sites rises to a maximum at about 12.6 wt% and then declines. This pattern is very similar to previously reported studies, in which the appearance of a maximum in the surface concentration of Brønsted-acid sites at a tungsten weight loading of 12.6 wt% was attributed to the formation of a polytungstate monolayer [28,31,40]. Fig. 2b demonstrates that the surface area also reaches a maximum at a tungsten weight loading of 12.6%. This effect is attributed to the fact that the addition of tungsten oxide inhibits the sintering of zirconia to the denser monoclinic phase,

Table 1
Screening of acid catalysts for the etherification of 1-dodecanol to di-n-dodecyl ether.

Entry	Acid catalyst	Dodecanol conversion (%)	Selectivity to ether (%)	Selectivity to alkenes/other (%)
1	Zeolite Beta	5	61	39
2	Para-Toluene Sulfonic Acid	3	40	60
3	Amberlyst 15	4	46	54
4	Amberlyst 36	6	65	35
5	Amberlyst 70	11	97	3
6	Nafion NR-50	10	98	2
7	WO_x/ZrO_2 (12.6 wt% W)	14	94	6
8	ZrO_2, Amorphous	0	0	0
9	ZrO_2, Monoclinic	0	0	0
10	Gamma-Alumina	0	0	0
11	Mesostructured Silica	0	0	0
12	Mesostructured Aluminosilicate	0	0	0

Reaction Conditions: 393 K, 4 h, 600 RPM, 500 mg 1-dodecanol, 150 mg n-tetradecane as internal standard. Entry 1: $3.3 * 10^{-5}$ mol eq. H+ acid sites, entries 2–5: $1*10^{-4}$ mol eq. H+ acid sites, entry 6: 0.043 g. cat, entry 7: $9.1*10^{-6}$ mol eq. H+ sites, entries 8–12: 100 mg catalyst.

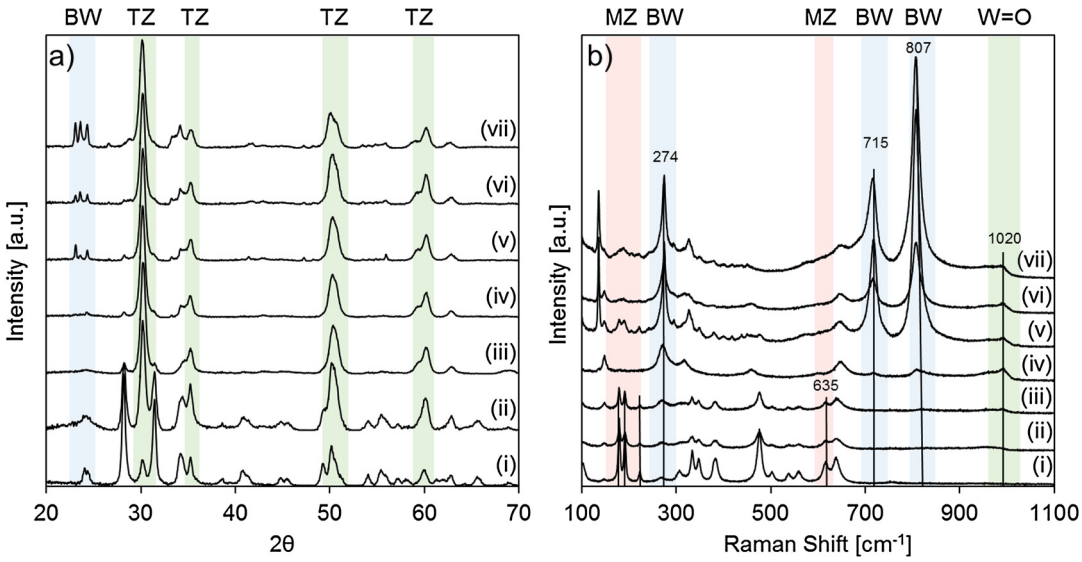

Fig. 1. (a) X-ray diffraction spectra of catalysts with tungsten weight loadings of (i) 0% (ii) 4.1%, (iii) 7.7%, (iv) 10.2%, (v) 12.6%, (vi) 15.4%, and (vii) 22.3%. (b) Raman spectra of catalysts with tungsten weight loadings of (i) 0%, (ii) 4.1%, (iii) 7.7%, (iv) 10.2%, (v) 12.6%, (vi) 15.4%, and (vii) 22.3%. Abbreviations: monoclinic zirconia (MZ), bulk WO_3 (BW), tetragonal zirconia (TZ).

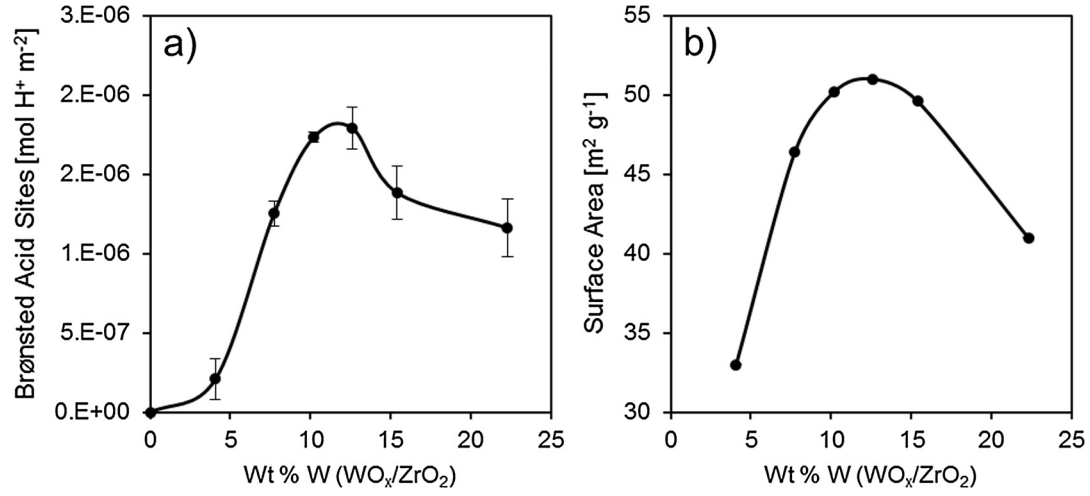

Fig. 2. (a) Brønsted-acid site density [mol H^+ m^{-2}] versus W weight loading [%], (b) Surface area [m^2 g^{-1}] versus W weight loading [%].

resulting in a higher surface area [41,42]. However, once the monolayer of polymeric tungsten oxide is exceeded, the formation of bulk WO_3 increases the mass of the catalyst but does not provide any additional active surface area, and is thus responsible for the decrease in surface area per mass of catalyst for the 15% and 22% W catalysts. The BET surface area, the concentration of Brønsted-acid sites, and the ratio of Brønsted- to Lewis-acid sites as functions of W weight loading are given in Table 2. The DRIFTS spectra of adsorbed pyridine used to determine the ratio of Brønsted- to Lewis-acid sites on the 4–22 wt% catalysts are provided in Fig. S4 of the Supporting Information.

The surface concentrations of active Brønsted- and Lewis-acid sites can be determined by poisoning them with a strongly bound adsorbate. DRIFTS spectra of adsorbed pyridine were obtained and used to determine the ratio of Brønsted- to Lewis-acid sites for the 4–22 wt% catalysts. As observed in Fig. 3a for the 12.6 wt% catalyst, bands at 1609 and 1444 cm^{-1} indicate the presence of Lewis-acid sites, and bands at 1639 and 1540 cm^{-1} indicate the presence of Brønsted acid sites upon addition of pyridine [30,43]. Extinction coefficients published by Emeis were used to determine the ratio of Brønsted- to Lewis-acid sites from the intensities of the bands at 1444 cm^{-1} and 1540 cm^{-1} [44]. As shown in Table 2, the ratio of Brønsted- to Lewis-acid sites increases with increasing weight loading of W until 12.6 wt%, beyond which the ratio decreases. Below 12.6 wt% W the Lewis-acid sites come from both tungsten and zirconia, but above 12.6 wt% W the Lewis-acid sites are predominately from tungsten. The decrease in the ratio of Brønsted-

Table 2
Characterization of 4–22 wt% W/ WO_X/ZrO_2.

Weight loading of W (wt% W, WO_x/ZrO_2)	BET Surface Area (m^2 g^{-1})	Brønsted Acid Sites (mol eq. H^+ m^{-2})	Ratio of Brønsted/ Lewis Acid Sites (393 K)
4.1	33	$2.09 * 10^{-7} \pm 1.2 * 10^{-7}$	0.33 ± 0.01
7.7	46	$1.26 * 10^{-7} \pm 6.5 * 10^{-8}$	0.57 ± 0.24
10.2	50	$1.74 * 10^{-6} \pm 4.0 * 10^{-8}$	0.92 ± 0.05
12.6	51	$1.78 * 10^{-6} \pm 1.4 * 10^{-7}$	0.90 ± 0.02
15.4	50	$1.38 * 10^{-6} \pm 1.6 * 10^{-7}$	0.30 ± 0.11
22.3	41	$1.17 * 10^{-6} \pm 1.7 * 10^{-7}$	0.28 ± 0.04

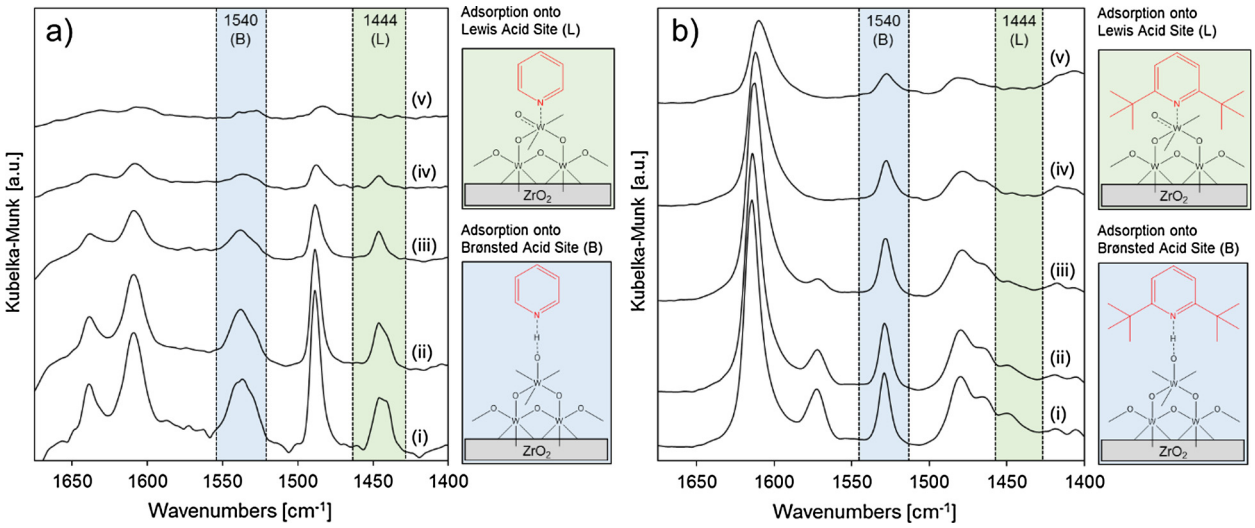

Fig. 3. (a) DRIFTS spectra for the adsorption of pyridine onto WO_x/ZrO_2 (12.6 wt% W) at (i) 393 K, (ii) 423 K, (iii) 473 K, (iv) 523 K, and (v) 573 K. (b) DRIFTS spectra for the adsorption of 2,6-di-tert-butyl-pyridine onto WO_x/ZrO_2 (12.6 wt% W) at (i) 393 K, (ii) 423 K, (iii) 473 K, (iv) 523 K, and (v) 573 K. Intensities normalized by the Kubelka-Munk function.

to Lewis-acid sites above 12.6 wt% is attributed to the formation of bulk tungsten oxide, as suggested by the structural characterization.

Pyridine poisons both Brønsted- and Lewis-acid sites, whereas 2,6-di-tert-butyl pyridine, a hindered base, will only poison Brønsted-acid sites [45]. Fig. 3b shows the diffuse reflectance infrared spectra for 2,6-di-tert-butyl pyridine adsorbed on the 12.6 wt% W catalyst. The spectrum of adsorbed pyridine in Fig. 3a exhibits bands at 1540 cm^{-1} and 1444 cm^{-1}, attributable to pyridine interacting with Brønsted- and Lewis-acid sites, respectively. By contrast, the spectrum for adsorbed 2,6-di-tert-butyl pyridine, shown in Fig. 3b, only exhibits a band at 1540 cm^{-1} for pyridine adsorption onto Brønsted-acid sites, but the band at 1444 cm^{-1} for pyridine adsorption onto Lewis-acid sites is absent.

3.3. Mechanisms and kinetics of dodecanol etherification and dehydration

A number of mechanisms have been proposed to explain the etherification and dehydration of alcohols over heterogeneous acid catalysts; these include dual-site Langmuir-Hinshelwood type mechanisms, Eley-Rideal type mechanisms with only one adsorbed alcohol, and mechanisms with more complex dimers and trimers of adsorbed reactants and products. Cunill et al. have proposed a modified Eley-Rideal model for the Brønsted-acid catalyzed liquid-phase etherification of 1-hexanol over Amberlyst 70 in which water remains adsorbed on the catalyst surface and, therefore, competes with the alcohol for acid sites [17]. Bhan et al. have proposed that the gas-phase etherification of ethanol over the Lewis-acidic γ-Al_2O_3 is inhibited by alcohol-water dimers on the catalyst surface [46]. Iglesia et al. have proposed that the gas-phase dehydration of ethanol over polyoxometalates involves adsorbed dimer and trimer species [47]. In the case of tungstated zirconia, different authors have claimed that the active centers for alcohol dehydration are Lewis- or Brønsted-acid sites. Larsen et al. have proposed that the dehydration of 1-propanol, 2-propanol, and tert-butanol over tungstated zirconia proceeds solely over Lewis-acid sites [27], whereas Iglesia et al. have proposed that 2-butanol dehydration occurs only over Brønsted-acid sites [28]. Theoretical and experimental evidence for synergistic effects between Lewis- and Brønsted-acid sites have also been suggested for metal oxide catalysis in the etherification of glycerol and other biomass-derived alcohols [48,49]. As discussed below, we propose that the mechanism for liquid-phase dodecanol etherification over tungstated zirconia that is most consistent with the kinetics reported here involves both Brønsted- and Lewis-acid sites and that the mechanism of dodecanol dehydration involves only Brønsted-acid sites.

The proposed mechanisms for etherification and dehydration of dodecanol over tungstated zirconia are shown in Scheme 1. We envision that the first step for both etherification and dehydration is the reversible adsorption of the alcohol onto a Brønsted-acid site. While the alcohol in Scheme 1 is shown as molecularly adsorbed, it is possible that it may adsorb dissociatively to form alkoxide species [46,50]; however, the differentiation between associative and dissociative adsorption was not considered in the present study. For etherification, the second alcohol molecule is assumed to adsorb onto an adjacent Lewis-acid site, and the rate-limiting step (RLS) is taken to be the reaction of the two adsorbed species to form adsorbed water and ether, which then desorb in the final step. The rate-limiting step for dehydration is the reaction of an alcohol molecule adsorbed at a Brønsted-acid site with a vacant basic site adjacent to the Brønsted-acid site, resulting in the abstraction of a hydrogen atom from the β-carbon of the adsorbed alcohol. The final step in the dehydration pathway is the desorption of water. As will be discussed below, ether and water can inhibit the rates of dodecanol etherification and dehydration.

To identify the rate-limiting steps for the liquid-phase etherification and dehydration of dodecanol, experiments were carried out using deuterium-labeled alcohols. The catalyst for these experiments was WO_x/ZrO_2 (12.6 wt% W). NMR was used to identify which H(D) atoms are involved in each reaction. Dehydration and etherification reactions of deuterium-labeled 1-hexanol (hexan-1,1-d_2-1-ol and hexan-2,2-d_2-1-ol) were used to probe the movement of hydrogen atoms on the α and β carbons of the alcohol. ^{1}H NMR of the ether and alkene products of the hexan-2,2-d_2-1-ol reaction showed no evidence of hydrogen on the β-carbon of the alkene, and no hydrogen present on either of the β-carbons of the ether. These results indicate that the hydrogens on the β-carbon are not involved in etherification, but are involved in the irreversible dehydration step. Also, the ^{1}H NMR of the products from the reaction of hexan-1,1-d_2-1-ol showed no change in the position of deuterium atoms on the α-carbon. In both deuterated alcohols, the lack of D/H scrambling indicates that etherifica-

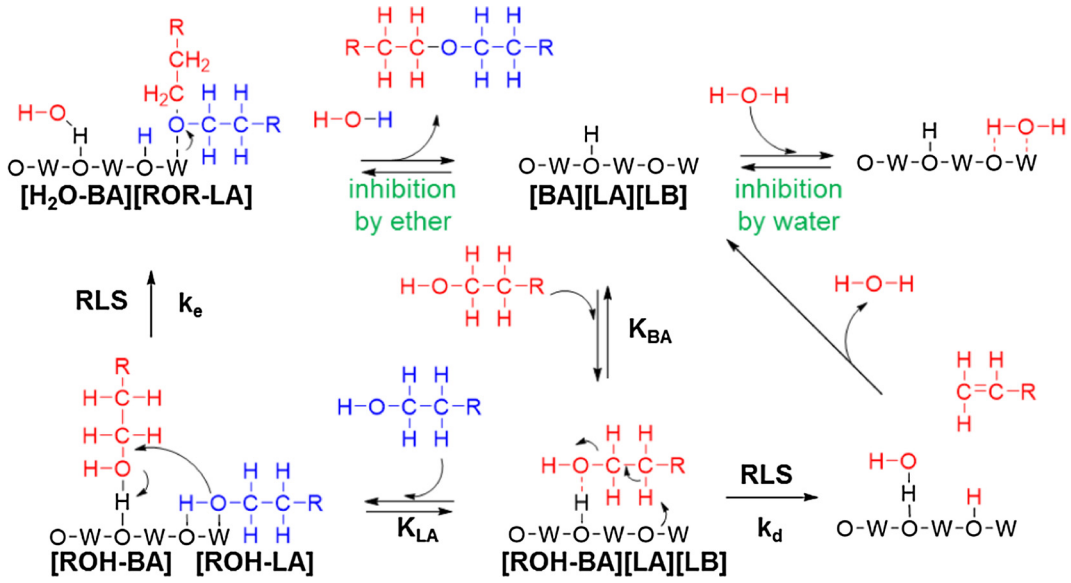

Scheme 1. Proposed mechanism for liquid phase primary linear alcohol etherification and unimolecular dehydration over tungstated zirconia.

Table 3
Measured kinetic isotope effects for hexene and di-n-hexyl ether synthesis at 418 K for the dehydration of hexan-1,1-d_2-1-ol and hexan-2,2-d_2-1-ol.

Product	Reactant	
	hexan-1,1-d_2-1-ol	hexan-2,2-d_2-1-ol
Di-n-Hexyl Ether KIE (k_H/k_D)	1.00 ± 0.09	1.03 ± 0.08
Hexene KIE (k_H/k_D)	1.01 ± 0.09	1.64 ± 0.09

tion and dehydration are irreversible under the conditions of the experiment. The NMR spectra are provided in Figs. S5a–S5f in the supporting information.

Measurement of kinetic isotope effects was used to confirm that the rate-limiting step for 1-hexanol dehydration is cleavage of the β-carbon C—H bond. Table 3 shows that there is a kinetic isotope effect for unimolecular dehydration of hexan-2,2-d_2-1-ol to form hexene (k_H/k_D = 1.64 ± 0.09), but there is no kinetic isotope effect for bimolecular etherification to form di-hexyl ether (k_H/k_D = 1.03 ± 0.08), confirming that the rate limiting step for alkene formation is β-carbon hydrogen bond cleavage. No kinetic isotope effect was observed for etherification or unimolecular dehydration reactions over hexan-1,1-d_2-ol, confirming that the α carbon-hydrogen bond is not involved in the rate limiting step. Therefore, the rate limiting step for etherification must involve either formation of the C—O bond or desorption of the ether from the acid site. This finding is in agreement with the results of Bhan et al., who used kinetic isotope effects to confirm that the β-carbon hydrogen bond cleavage was the rate limiting step for unimolecular dehydration of propanol over γ-Al_2O_3 [51].

The kinetics of dodecanol etherification and dehydration based on Scheme 1 involve the equilibrium adsorption of alcohol on Brønsted- and Lewis-acid sites and the rates of the reactions leading to alcohol etherification and dehydration. These relationships are given by Eqs. (1)-(4):

$$[ROH] + [BA] \overset{K_{BA}}{\leftrightarrow} [ROH - BA] \tag{1}$$

$$[ROH] + [LA] \overset{K_{LA}}{\leftrightarrow} [ROH - LA] \tag{2}$$

$$r_e = k_e[ROH - LA][ROH - BA] \tag{3}$$

$$r_d = k_d[ROH - BA][LB] \tag{4}$$

Substitution of Eqs. (1) and (2) into Eqs. (3) and (4) gives:

$$r_e = k_e K_{LA} K_{BA}[ROH]^2[LA][BA] \tag{5}$$

$$r_d = k_d K_{BA}[ROH][BA][LB] \tag{6}$$

The overall rates of etherification and dehydration based on this set of elementary steps and site balances on the Brønsted-acid sites [BA], Lewis-acid sites [LA], and Lewis-base sites [LB] are given by the following expressions (see Supporting Information for the derivation of these expressions):

$$r_e = \frac{k_e K_{LA} K_{BA}[ROH]^2}{(1 + K_{BA}[ROH] + K_{ROR-BA}[ROR] + K_{H2O-BA}[H_2O])(1 + K_{LA}[ROH] + K_{ROR-LA}[ROR] + K_{H2O-LA}[H_2O])} \tag{7}$$

$$r_d = \frac{k_d K_{BA}[ROH]}{(1 + K_{BA}[ROH] + K_{ROR-BA}[ROR] + K_{H2O-BA}[H_2O])(1 + K_{LB}[ROH] + K_{ROR-LB}[ROR] + K_{H2O-LB}[H_2O])} \tag{8}$$

In Eqs. (7) and (8), k_e is the rate coefficient for the rate-limiting step of etherification, K_{LA} is the equilibrium constant for adsorption of an alcohol onto a Lewis-acid site, K_{BA} is the equilibrium constant for adsorption of an alcohol onto a Brønsted-acid site, $K_{ROR\text{-}BA}$ is the equilibrium constant for ether adsorption onto a Brønsted-acid site, $K_{H2O\text{-}BA}$ is the equilibrium constant for water adsorption onto a Brønsted-acid site, $K_{ROR\text{-}LA}$ is the equilibrium constant for ether adsorption onto a Lewis-acid site, $K_{H2O\text{-}LA}$ is the equilibrium constant for water adsorption onto a Lewis-acid site, k_d is the rate constant for the rate-limiting step of dehydration, K_{LB} is the equilibrium constant for adsorption of an alcohol onto a basic site, $K_{ROR\text{-}LB}$ is the equilibrium constant for adsorption of an ether onto a basic site, and $K_{H2O\text{-}LB}$ is the equilibrium constant for adsorption of water onto a basic site. For low conversions where [ROR] and [H_2O] are negligible, and with the assumption that the Brønsted-acid sites are saturated with reactant (K_{BA}[ROR] ≫ 1), Eqs. (7) and (8) simplify to:

$$r_e = \frac{k_e K_{LA}[ROH]}{1 + K_{LA}[ROH]} \quad (9)$$

$$r_d = \frac{k_d}{1 + K_{LB}[ROH]} \quad (10)$$

3.4. Rates of dodecanol etherification and dehydration

The effect of alcohol concentration on the initial rates of etherification and dehydration was determined by measuring the initial rates of di-dodecyl ether and dodecene formation at varying initial concentrations of dodecanol in decane over a temperature range of 388–403 K, and the results are shown in Fig. 4. The solid curves in these figures represent a fit to the data by Eqs. (9) and (10). The rate coefficients and equilibrium constants required to achieve these fits are given in Table 4. It is clear from Fig. 4a and b, and from the parity plots shown in Fig. 4c and d, that there is good agreement between the predicted and observed rates for ether and alkene formation for temperatures between 388 and 403 K.

The rate coefficients and equilibrium constants k_e, k_d, K_{LA}, and K_{LB} and the respective activation energies and enthalpies of adsorption were determined from Arrhenius and Van't Hoff plots (Supporting Information, Fig. S2), and the values of these parameters are given in Table 4. The apparent activation energy for etherification (128 kJ mol^{-1}), is significantly lower than the activation energy for unimolecular dehydration (152 kJ mol^{-1}). The value of the apparent activation energy for etherification lies in the range of values reported for liquid-phase etherification of 1-hexanol and 1-octanol over other solid acid catalysts such as H-BEA, Amberlyst 70, and Nafion NR-50, which range from 118 to 150 kJ mol^{-1} [17,19,20]. The unimolecular dehydration activation barrier also falls within the range of values reported for the dehydration of linear alcohols over solid acids such as TiO_2, ZrO_2, and γ-Al_2O_3, which range from 141 to 171 kJ mol^{-1}.[52,53] The relatively high activation barrier for unimolecular dehydration compared to etherification observed in this study over tungstated zirconia

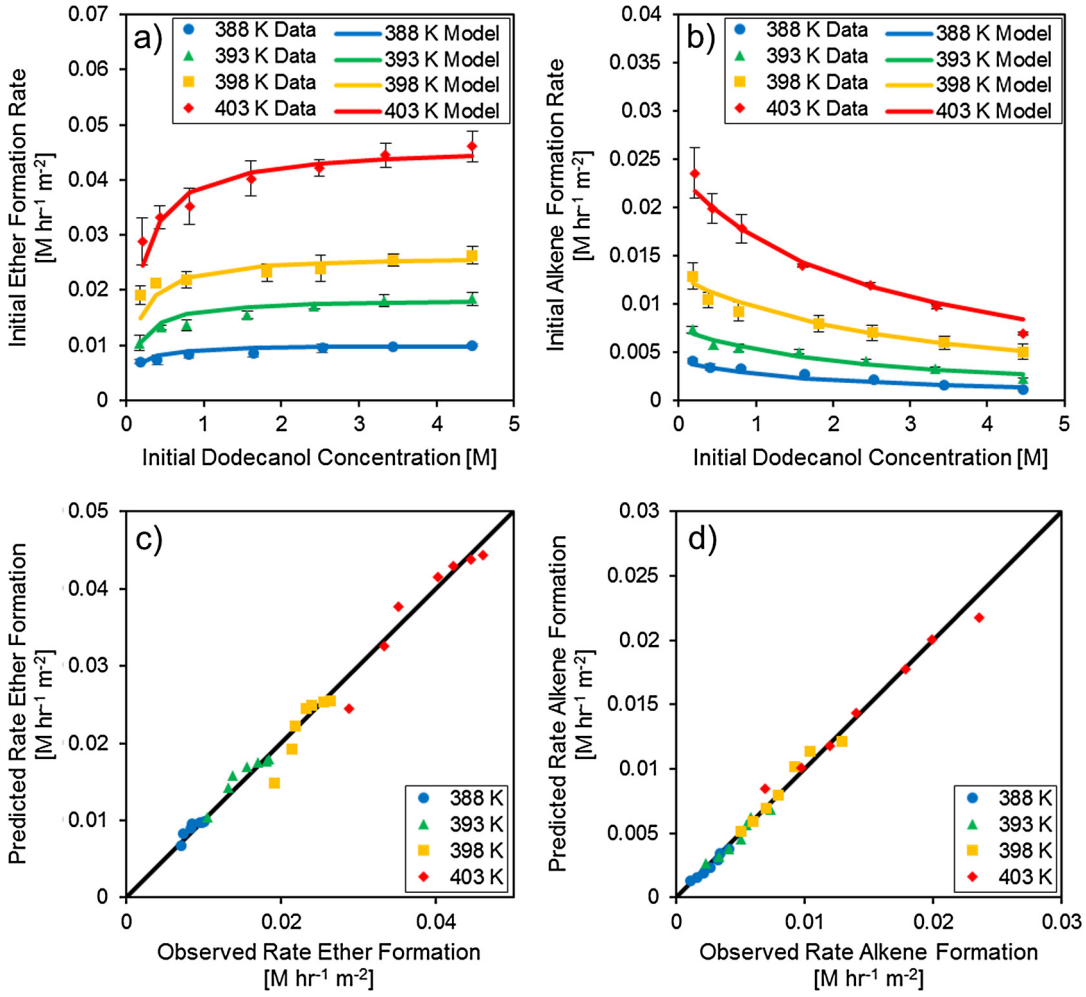

Fig. 4. (a) Effect of initial dodecanol concentration in decane [M] on initial rates of di-dodecyl ether formation [M h^{-1} m^{-2}], (b) effect of initial dodecanol concentration in decane [M] on initial rates of dodecene formation [M h^{-1} m^{-2}] for reactions from 388 to 403 K with 100 mg WO_x/ZrO_2 (12.6 wt% W) and a reaction volume of 2.4 * 10^{-4} L, (c) parity plot for ether formation, and (d) parity plot for alkene formation.

Table 4
Kinetic parameters.

Temperature [K]	k_e [M h^{-1} m^{-2}]	k_d [M h^{-1} m^{-2}]	K_{LA} [M^{-1}]	K_{LB} [M^{-1}]
388	0.010	0.004	11.5	0.459
393	0.018	0.007	7.50	0.391
398	0.026	0.013	7.06	0.341
403	0.046	0.024	5.53	0.400
E_a [kJ mol^{-1}]	128 ± 8	152 ± 2		
ln[A] [M h^{-1} m^{-2}]	35 ± 3	42 ± 1		
ΔH_{ads} [kJ mol^{-1}]			−59 ± 12	−15 ± 14
ΔS [J mol^{-1} K^{-1}]			−132 ± 31	−44 ± 35

explains the higher selectivity to ether in the liquid phase than the gas phase.

3.5. Inhibition of dodecanol etherification and dehydration by water and ether

Water has been shown to inhibit Brønsted-acid sites during the liquid-phase etherification of 1-hexanol over Amberlyst 70 [17], and it is reasonable to expect that ether may have a similar inhibitory effect. To assess the influence of water and ether on the rates of etherification and dehydration of dodecanol, the initial rates of ether and alkene formation were measured at 393 K with varying initial concentrations of water and ether added to the reactor. To distinguish between ether added initially and ether formed, di-decyl ether was used for ether inhibition experiments instead of di-dodecyl ether. The results indicate that water inhibits both ether and alkene formation, while the di-decyl ether only inhibits ether formation and not dehydration. These data are given in the Supporting Information, Fig. S3. With the assumption that saturation of Brønsted-acid sites is unaffected by the presence of water and ether, but ether and water inhibit adsorption on Lewis-acid and base sites, the rate expressions for etherification and dehydration now become:

$$r_e = \frac{k_e K_{LA}[ROH]}{(1 + K_{LA}[ROH] + K_{ROR-LA}[ROR] + K_{H2O-LA}[H_2O])} \quad (11)$$

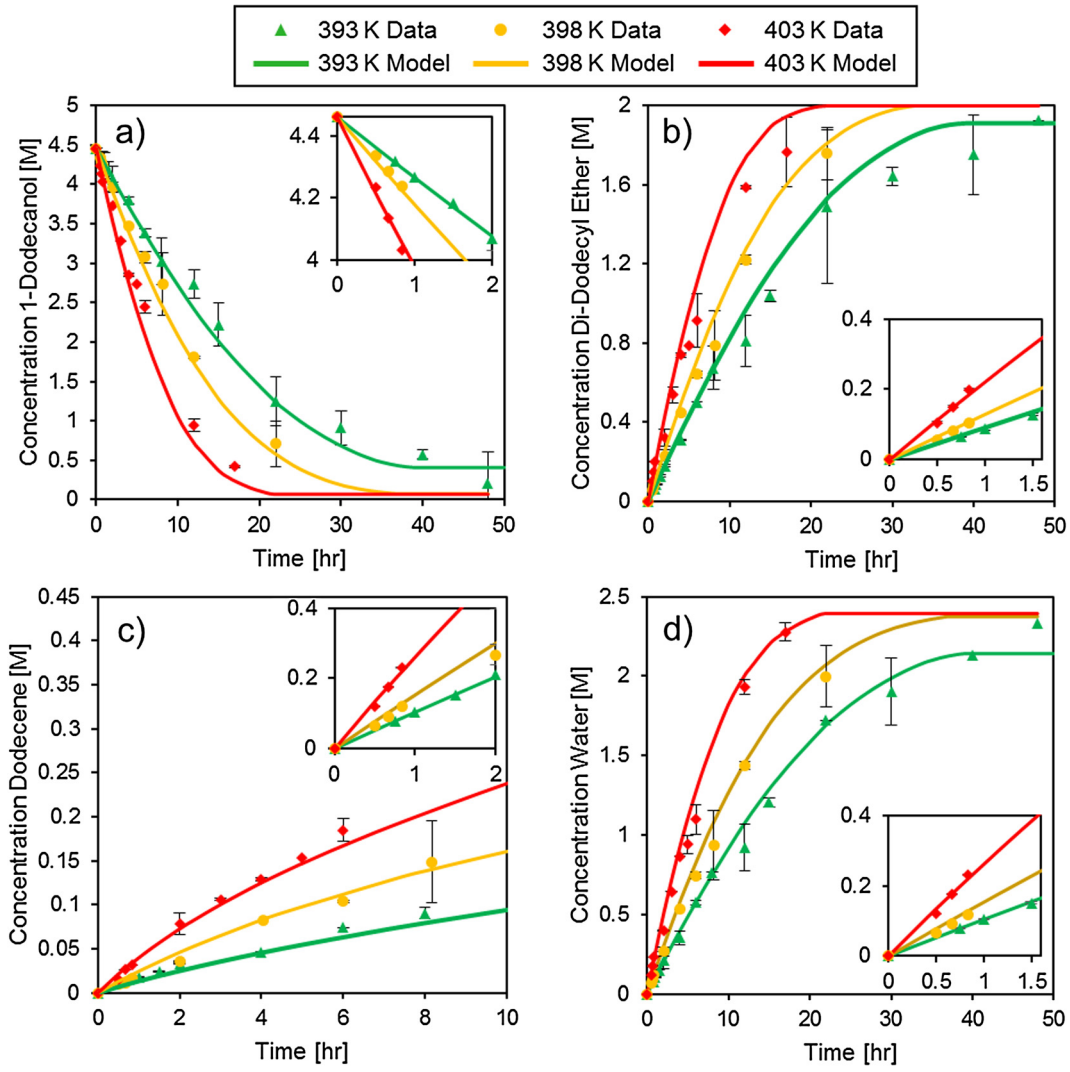

Fig. 5. Concentration [M] versus time [h] for experimental data and model from 393 K – 403 K for (a) 1-dodecanol, (b) di-dodecyl ether, (c) dodecene, and (d) water over WO_x/ZrO_2 (12.6 wt% W). Linear portions of the time-course curves for low conversions are shown in the insets.

$$r_d = \frac{k_d}{(1 + K_{LB}[ROH] + K_{ROR-LB}[ROR] + K_{H2O-LB}[H_2O])} \quad (12)$$

The values of the rate coefficients and equilibrium constants appearing in Eqs. (11) and (12), k_e, k_d, K_{LA}, and K_{LB}, were fixed at the values given in Table 4 and the equilibrium constants K_{ROR-LA}, K_{H2O-LA}, K_{ROR-LB}, and K_{H2O-LB} were then fitted to the data using the following constraints: First, the value of K_{ROR-LB} was taken to be approximately equal to 0 based on ether-inhibition experiments indicating that ether only inhibits the rate of etherification. Second, when considering acid site balances over both Lewis-acid sites and Lewis-base sites, it was assumed that water adsorbs onto an acid-base pair; therefore, K_{H2O-LA} must be equal to K_{H2O-LB}. Finally, inhibition studies suggested that water has a greater inhibiting effect on both reactions, implying that $K_{ROR-LA} < K_{H2O-LA}$ and K_{H2O-LB}. Using these constraints, data for the complete conversion of pure dodecanol at 393 K, 398 K, and 403 K was used to estimate values for K_{ROR-LA}, K_{H2O-LA}, and K_{H2O-LB}. The experimental curves for concentration of reactants and products versus time and the fits of the model to these data are shown in Fig. 5. The equilibrium constants and adsorption energies obtained in this manner are shown in Table 5.

3.6. Role of Brønsted- and Lewis-acid sites

The role of the Brønsted-acid sites was probed by examining the relationship between reaction rates and Brønsted-acid site density, whereas poisoning experiments were used to probe the roles of both Brønsted- and Lewis-acid sites.

Initial rates of etherification and dehydration were measured over tungstated zirconia with varying Brønsted-acid site densities. The initial rates of etherification and dehydration across the 4–22 wt% catalysts are shown in Fig. 6a. The rates of etherification and dehydration peak between 10.2 and 12.6 wt% W, where the Brønsted acid site density reaches a maximum. It is clear from Fig. 6b that the initial rates of 1-dodecanol etherification and dehydration have a nearly linear relationship with Brønsted-acid site density and that the selectivity to ether does not change significantly with Brønsted-acid site density. Characterization of the catalysts (see Table 2) indicates that the ratio of Brønsted- to Lewis-acid sites changes with weight loading of tungsten, suggesting that the selectivity to ether is independent of the ratio of Brønsted- to Lewis-acid sites. However, as the Brønsted-acid site density increases, so does the fraction of Lewis-acid sites attributed to W, thus the rate of reaction may also increase with increasing W Lewis-acid site density.

As demonstrated from the DRIFTS characterization in Fig. 3a and b, pyridine poisons both Brønsted- and Lewis-acid sites, whereas 2,6-di-tert-butyl pyridine poisons only Brønsted acid sites. To test the effects of acid-site poisoning on the rates of ether and alkene formation, the initial rates of etherification and dehydration were measured for reactions with different initial concentrations of pyridine or 2,6-di-tert-butyl pyridine added to the reaction mixture. These results are shown in Fig. 7. The rate of ether formation is observed to decrease as the concentration of the base increases, with the decrease in the rate being somewhat smaller for pyridine than for 2,6-di-tert-butyl pyridine poisoning. These results clearly demonstrate that both poisons are effective in blocking the adsorption of alcohol onto Brønsted-acid sites, a critical initial step for etherification.

Because the Brønsted- to Lewis-acid site ratio for WO_x/ZrO_2 (12.6 wt% W) is approximately 0.9, if Lewis-acid sites were not at all active in the etherification reaction, we would predict that approximately 1.8 mol of pyridine would be necessary to achieve the same decrease in rate as 1 mol of 2,6-di-tert-butyl pyridine. However, for this reaction, the decrease in the etherification rate is nearly the same for pyridine and hindered pyridine. This observation is consistent with the proposed mechanism, indicating that both Brønsted- and Lewis-acid sites play a role in the etherification reaction. Upon poisoning both Brønsted- and Lewis-acid sites with pyridine, the rate of ether formation reaches zero; however, after poisoning only the Brønsted-acid sites on the surface with hindered pyridine, some ether formation can still occur. This suggests that the Lewis-acid sites may be active for etherification on their own. The fact that Lewis-acid sites are still active supports the hypothesis that the surface is dominated by W Lewis-acid sites as opposed to Zr Lewis-acid sites because zirconia itself is not active for etherification (Table 1, entries 8–9). We also note that

Table 5
Kinetic parameters for water and ether inhibition.

Temperature [K]	K_{ROR-LA} [M^{-1}]	K_{H2O-LA} [M^{-1}]	K_{H2O-LB} [M^{-1}]
393	3	4	4
398	2.95	3.8	3.8
403	2.9	3.6	3.6
ΔH [kJ mol^{-1}]	−4	−14	−14
ΔS [J mol^{-1} K^{-1}]	−2.2 ± 0.14	−44 ± 35	−24 ± 0.78

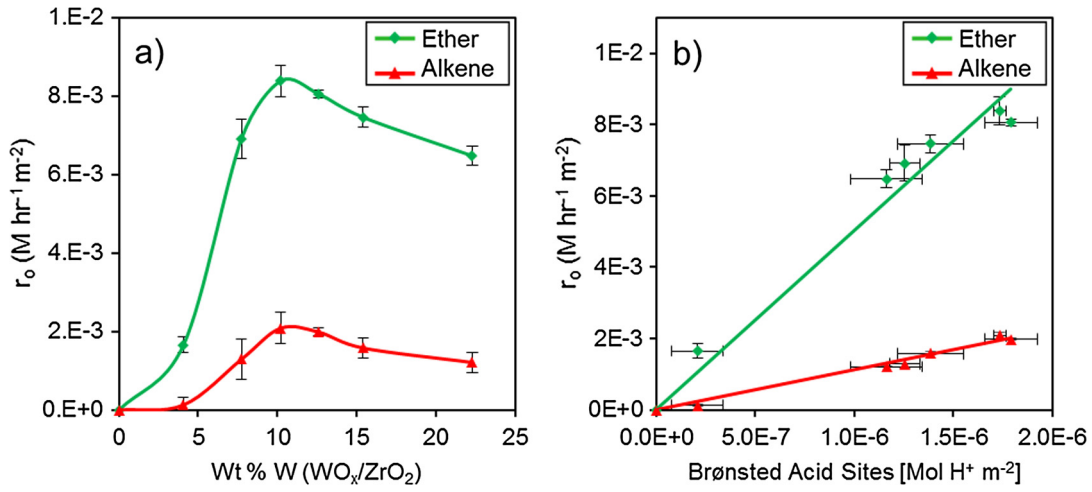

Fig. 6. (a) Initial rates of ether and alkene formation [M h^{-1} m^{-2}] versus W weight loading, (b) Brønsted-acid site density [mol H^+ m^{-2}] versus rates of ether and alkene formation [M h^{-1} m^{-2}]. Reaction conditions: 393 K, 100 mg WO_x/ZrO_2 (12.6 wt% W), 600 RPM.

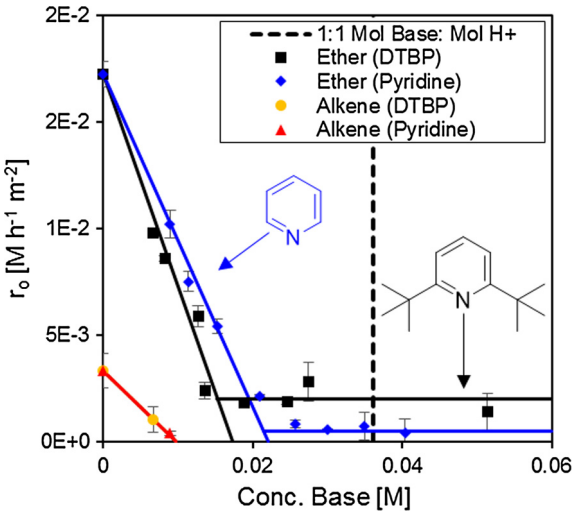

Fig. 7. Initial rates of ether formation [M h^{-1} m^{-2}] with varying initial concentrations [M] of 2,6-di-tert-butyl pyridine (DTBP) (black square) and pyridine (blue diamond), and initial rates of alkene formation with varying initial concentrations of DTBP (orange circle) and pyridine (red triangle).

no alkene is formed once all of the Brønsted-acid sites are poisoned, consistent with the proposed mechanism. Based on the proposed mechanism and the resulting expressions for the reaction rates, we anticipate that the overall selectivity to ether would decrease if the tungsten Lewis-acid sites could be poisoned without altering the Brønsted-acid site density.

The dotted vertical line in Fig. 7 represents the concentration of base equal to the measured concentration of Brønsted-acid sites determined by base titration. There are several possible reasons why the concentration of Brønsted-acid sites measured by ion exchange and titration is not equal to the concentration of hindered pyridine at which the rate becomes zero. First, given that there is a distribution in acid site strength, there may be some acid sites that are not active for etherification or dehydration. Second, the presence of a base on a Brønsted- or Lewis-acid site may alter the acidity of adjacent Lewis- or Brønsted-acid sites, respectively. Finally, there may be steric factors responsible for the enhanced decrease in rate. Bond lengths for W—O are on the order of 2 angstroms, and O—H bonds are on the order of 0.8 angstroms [54], while the width of pyridine is on the order of 2.8 angstroms [55], making it possible that a single pyridine molecule could inhibit multiple acid sites.

4. Conclusions

Tungstated zirconia is shown to be active and highly selective for the etherification of 1-dodecanol. It is proposed that the mechanism for liquid-phase etherification of 1-dodecanol over this catalyst involves a cooperation between Brønsted- and Lewis-acid sites that facilitates the bi-molecular etherification reaction. Isotopic labeling studies suggest that the rate-limiting step for etherification involves the formation of a carbon oxygen bond between two adsorbed alcohol molecules, and that the rate-limiting step for dehydration is the cleavage of the bond between the β-carbon and a hydrogen atom in an adsorbed alcohol. The proposed mechanism suggests that both etherification and dehydration require alcohol adsorption onto a Brønsted-acid site and that etherification requires an additional alcohol adsorbed onto an adjacent W Lewis-acid site, while dehydration requires an open Lewis base site. A kinetic model based on the proposed mechanism (Scheme 1) was developed and fitted to initial reaction rate data for etherification and dehydration. This model was then modified to include the inhibiting effects of ether and water on both reactions. It was found that the rates of etherification and dehydration correlate linearly with Brønsted-acid site density, supporting the hypothesis that both reactions require Brønsted-acid sites. Due to the absence of activity for etherification over pure zirconia, and the relationship between tungsten oxide weight loading and reaction rate, it was concluded that the active Lewis-acid sites are associated with the dispersed tungsten oxide as opposed to zirconia. Poisoning of the catalyst with pyridine and hindered pyridine indicates that Lewis-acid sites are active for etherification but not dehydration, which is consistent with the proposed mechanism.

Acknowledgements

This work was funded by the Energy Biosciences Institute. J. Rorrer would also like to acknowledge funding from the National Science Foundation Graduate Research Fellowship under Grant No. DGE 1106400. The authors thank Chris Ho, Lin Louie, and Joaquin Resasco for assistance with XRD, FTIR, and Raman spectroscopy, respectively. The authors also thank Adam Grippo, Konstantinos Goulas, and Miriam Eulers for useful discussion, and Alan Liu for assisting in reaction preparation.

Appendix A. Supplementary material

Supplementary data associated with this article can be found, in the online version, at http://dx.doi.org/10.1016/j.jcat.2017.08.001.

References:

[1] L. Chapman, J. Transp. Geogr. 15 (2007) 354–367.
[2] G.W. Huber, S. Iborra, A. Corma, Chem. Rev. 106 (2006) 4044–4098.
[3] M. Balakrishnan, E.R. Sacia, S. Sreekumar, G. Gunbas, A.A. Gokhale, C.D. Scown, F.D. Toste, A.T. Bell, Proc. Natl. Acad. Sci. 112 (2015) 7645–7649.
[4] C. Carlini, A. Macinai, A.M. Raspolli Galletti, G. Sbrana, J. Mol. Catal. A Chem. 212 (2004) 65–70.
[5] R.J.J. Nel, A. De Klerk, Ind. Eng. Chem. Res. 48 (2009) 5230–5238.
[6] M.J. Truitt, Condensation of Alcohols for Biofuel Production, US 8845766 B2, 2014.
[7] A.L. Maximov, A.I. Nekhaev, D.N. Ramazanov, Pet. Chem. 55 (2015) 1–21.
[8] G. Olah, Cleaner Burning and Cetane Enhancing Diesel Fuel Supplements, US Patent 5520710 A, 1996.
[9] M.J. Pilling, Low-Temperature Combustion and Autoignition, Elsevier, 1997.
[10] K.W. Wolfgang Beilfuss, Ralf Gradtke, Wolfgang Siegert, Karl-Heinz Diehl, Glyceryl Ethers as Preservatives for Cooling Lubricants, US Patent 7268102 B2, 2007.
[11] D.A.L. Leslie, R. Rudnick, Ross A. Kremer, Alkylated Diphenyl Ether Lubricants, Patent US 5552071 A, 1996.
[12] L.R. Rudnick, Synthetics, Mineral Oils, and Bio-Based Lubricants: Chemistry and Technology, Second Edition., CRC Press, Taylor And Francis Group, Boca Raton, 2013.
[13] D. Jadhav, A.M. Grippo, S. Shylesh, A.A. Gokhale, J. Redshaw, A.T. Bell, ChemSusChem 10 (2017) 2527–2533.
[14] T. Zolper, Z. Li, C. Chen, M. Jungk, T. Marks, Y.-W. Chung, Q. Wang, Tribol. Lett. 48 (2012) 355–365.
[15] R. Benda, J. Bullen, A. Plomer, J. Synth. Lubr. 13 (1996) 41–57.
[16] M. Balakrishnan, E.R. Sacia, A.T. Bell, Green Chem. 14 (2012) 1626–1634.
[17] R. Bringué, E. Ramírez, M. Iborra, J. Tejero, F. Cunill, Chem. Eng. J. 246 (2014) 71–78.
[18] R. Bringué, M. Iborra, J. Tejero, J. Izquierdo, F. Cunill, C. Fite, V. Cruz, J. Catal. 244 (2006) 33–42.
[19] E. Medina, R. Bringué, J. Tejero, M. Iborra, C. Fité, Appl. Catal. A Gen. 374 (2010) 41–47.
[20] I. Hoek, T.A. Nijhuis, A.I. Stankiewicz, J.A. Moulijn, Appl. Catal. A Gen. 266 (2004) 109–116.
[21] K. Arata, Adv. Catal. 37 (1990) 165–211.
[22] G. Perot, M. Guisnet, J. Mol. Catal. 61 (1990) 173–196.
[23] M. Hino, K. Arata, J. Chem. Soc. Chem. Commun. (1988) 1259–1260.
[24] W. Zhou, N. Soultanidis, H. Xu, M.S. Wong, M. Neurock, C.J. Kiely, I.E. Wachs, ACS Catal. 7 (2017) 2181–2198.
[25] M.K. Patil, A.N. Prasad, B.M. Reddy, Curr. Org. Chem. 15 (2011) 3961–3985.
[26] D.E. López, K. Suwannakarn, D.A. Bruce, J.G. Goodwin, J. Catal. 247 (2007) 43–50.
[27] G. Larsen, E. Lotero, L.M. Petkovic, D.S. Shobe, J. Catal. 169 (1997) 67–75.

[28] J. Macht, C.D. Baertsch, M. May-Lozano, S.L. Soled, Y. Wang, E. Iglesia, J. Catal. 227 (2004) 479–491.
[29] S. Peng, N.M. Okeley, A.-L. Tsai, G. Wu, R.J. Kulmacz, W.A. Van der Donk, J. Am. Chem. Soc. 124 (2002) 10785–10796.
[30] Y. Zhao, W. Li, M. Zhang, K. Tao, Catal. Commun. 3 (2002) 239–245.
[31] C.D. Baertsch, S.L. Soled, E. Iglesia, J. Phys. Chem. B 105 (2001) 1320–1330.
[32] A. Wang, N.P. Balsara, A.T. Bell, Green Chem. 18 (2016) 4073–4085.
[33] J.A. Melero, J. Iglesias, G. Morales, Green Chem. 11 (2009) 1285–1308.
[34] S.R. Ginjupalli, S. Mugawar, P. Rajan, N., P. Kumar Balla, V. R. C. Komandur, J. Chem. Technol. Biotechnol. 89 (2014) 1890–1897.
[35] G. Larsen, E. Lotero, S. Raghavan, R.D. Parra, C.A. Querini, Appl. Catal. A Gen. 139 (1996) 201–211.
[36] D.G. Barton, S.L. Soled, G.D. Meitzner, G.A. Fuentes, E. Iglesia, J. Catal. 181 (1999) 57–72.
[37] R. Balzer, V. Drago, W.H. Schreiner, L.F.D. Probst, J. Braz. Chem. Soc. 25 (2014) 2026–2031.
[38] M. Li, Z. Feng, G. Xiong, P. Ying, Q. Xin, C. Li, J. Phys. Chem. B 105 (2001) 8107–8111.
[39] S. Kuba, P. Concepción Heydorn, R.K. Grasselli, B.C. Gates, M. Che, H. Knözinger, Phys. Chem. Chem. Phys. 3 (2001) 146–154.
[40] A. Galano, G. Rodriguez-Gattorno, E. Torres-García, Phys. Chem. Chem. Phys. 10 (2008) 4181–4188.
[41] K. Shimizu, T.N. Venkatraman, W. Song, Appl. Catal. A Gen. 225 (2002) 33–41.
[42] E.I. Ross-Medgaarden, W.V. Knowles, T. Kim, M.S. Wong, W. Zhou, C.J. Kiely, I.E. Wachs, J. Catal. 256 (2008) 108–125.
[43] R. Kourieh, S. Bennici, A. Auroux, React. Kinet. Mech. Catal. 105 (2012) 101–111.
[44] C.A. Emeis, J. Catal. 141 (1993) 347–354.
[45] C. Baertsch, K.T. Komala, Y. Chua, E. Iglesia, J. Catal. 205 (2002) 44–57.
[46] J.F. DeWilde, H. Chiang, D.A. Hickman, C.R. Ho, A. Bhan, ACS Catal. 3 (2013) 798–807.
[47] W. Knaeble, E. Iglesia, J. Phys. Chem. C 120 (2016) 3371–3389.
[48] G.S. Foo, D. Wei, D.S. Sholl, C. Sievers, ACS Catal. 4 (2014) 3180–3192.
[49] M. Calatayud, A.M. Ruppert, B.M. Weckhuysen, Chemistry 15 (2009) 10864–10870.
[50] A.J. Jones, E. Iglesia, Angew. Chemie Int. Ed. 53 (2014) 12177–12181.
[51] M. Kang, J.F. DeWilde, A. Bhan, ACS Catal. 5 (2015) 602–612.
[52] P. Kostestkyy, J. Yu, R.J. Gorte, G. Mpourmpakis, Catal. Sci. Technol. 4 (2014) 3861.
[53] S. Roy, G. Mpourmpakis, D. Hong, D.G. Vlachos, A. Bhan, R.J. Gorte, ACS Catal. 2 (2012) 1846–1853.
[54] J.T. Szymanski, A.C. Roberts, Can. Mineral. 22 (1984) 681–688.
[55] D. Mootz, H.G. Wussow, J. Chem. Phys. 75 (1981) 1517–1522.